A Preliminary 1D-3D Analysis of the Darmstadt Research Engine Under Motored Condition

Clara Iacovano[1,*], *Fabio* Berni[1], *Alessio* Barbato[1] and *Stefano* Fontanesi[1]

[1]Dipartimento di Ingegneria "Enzo Ferrari" (DIEF) University of Modena and Reggio Emilia, Via Vivarelli 10, 41125 Modena, Italy

Abstract. In the present paper, 1D and 3D CFD models of the Darmstadt research engine undergo a preliminary validation against the available experimental dataset at motored condition. The Darmstadt engine is a single-cylinder optical research unit and the chosen operating point is characterized by a revving speed equal to 800 rpm with intake temperature and pressure of 24 °C and 0.95 bar, respectively. Experimental data are available from the TU Darmstadt engine research group. Several aspects of the engine are analyzed, such as crevice modeling, blow-by, heat transfer and compression ratio, with the aim to minimize numerical uncertainties. On the one hand, a GT-Power model of the engine is used to investigate the impact of blow-by and crevices modeling during compression and expansion strokes. Moreover, it provides boundary conditions for the following 3D CFD simulations. On the other hand, the latter, carried out in a RANS framework with both high- and low-Reynolds wall treatments, allow a deeper investigation of the boundary layer phenomena and, thus, of the gas-to-wall heat transfer. A detailed modeling of the crevice, along with an ad hoc tuning of both blow-by and heat fluxes lead to a remarkable improvement of the results. However, in order to adequately match the experimental mean in-cylinder pressure, a slight modification of the compression ratio from the nominal value is accounted for, based on the uncertainty which usually characterizes such geometrical parameter. The present preliminary study aims at providing reliable numerical setups for 1D and 3D models to be adopted in future detailed investigations on the Darmstadt research engine.

1 Introduction

Energy saving and environmental protection are currently the main goals of the internal combustion engine research community. Such targets are achieved via an ad hoc design, aiming at increasing the efficiency and reducing the pollutant formation. As for the latter, in the last decades, the more and more stringent laws have been pushing on the one hand to the diffusion of hybrid (or even fully electric) vehicles [1,2] and on the other hand to a noticeable development of the spark-ignition engine. Focusing on gasoline engines, specific consumption reduction is mainly obtained promoting knock mitigation by means of

* Corresponding author : *Clara.iacovano@unimore.it*

different techniques, such as improved cooling [3], variable compression ratio [4], bore reduction [5], alternative valve strategies [6,7], cooled EGR, water or water/methanol injection [8-9], split injections [10] and increased injection pressures (up to several hundred bar to promote evaporation and mixing) [11]. In this panorama, a key-role is played by CFD simulations whose capabilities to predict knock onset, to understand its origin and to investigate other in-cylinder process (such as complex turbulent flow [12-16], injection [17,19], flame kernel development [20] and combustion [21]) are fundamental to guide design, thus saving costs and time [22-24]. Focusing on the field of internal combustion engine research, numerical investigations under motored conditions represent a common practice in order to evaluate the agreement between 1D/3D models and experiments [25].
However, before complex comparisons between numerical and experimental outcomes [26,27], the CFD models has to match global engine parameters such as intake mass flow rate, heat transfer and, mostly, mean in-cylinder pressure [28-32]. The latter is widely adopted both at motored and firing conditions as main indicator of the quality the numerical analysis. In fact, it is able to synthesize the effect of several aspects affecting the simulation such as compression ratio, trapped mass, blow-by and heat transfer.
As for the compression ratio, both piston position at the top dead center (TDC) and presence of a piston crevice can have a huge impact and its experimental evaluation is not straightforward [33]. In the industrial practice, crevice volume is often neglected for production engines, since it represents a small percentage of the TDC volume. Conversely, for optical research engines the crevice volume can be relevant, thus remarkably changing the compression ratio.
As for trapped mass, blow-by and heat transfer, only the first can be reliably estimated via the intake air flow rate measure. In fact, local heat flux measurements can be carried out, but they are not able to provide a full description of the heat transfer through the cylinder walls. Nonetheless, all the three parameters have a remarkable impact on the mean in-cylinder pressure.
The aim of the present work is a preliminary validation of 1D and 3D CFD models of the Darmstadt research engine against experiments at motored condition. In particular, validation is carried out in terms of global parameters, i.e. intake mass flow rate and mean in-cylinder pressure. In order to improve the agreement between numerical and experimental outcomes, all the aspects mentioned above are deeply investigated, that is compression ratio, trapped mass, blow-by mass flow and heat transfer (through both crevice and cylinder walls). The resulting 1D and 3D models represent a starting point for future analyses on the Darmstadt research engine.

2 Darmstadt Engine

The engine investigated was developed by the TU Darmstadt research group to study both cold flow, mixing and combustion. It is an optical accessible single-cylinder direct-injection spark-ignition engine with a 55 mm height quartz-glass cylinder liner and a flat quartz-glass piston. Bore and stroke are equal to 86 mm with a resulting displacement of 499 cm^3. Geometric compression ratio is 8.7. It is equipped with two different cylinder head configurations which differ for the position of the fuel-injector [27]. In the present study the spray-guided (SG) direct-injection configuration [34] has been considered in which the four-valve pent-roof cylinder head is provided with centrally-mounted fuel injector and spark plug (both inactive during motored experiments). Dual-port intake/exhaust systems are attached to the cylinder head and the intake valve configuration promotes tumble. The cylinder domain extends below the piston with crevice 77.6 mm long and 0.5 mm thick. This volume is included in the geometric compression ratio.

Experimental measurements are available at four motored operating conditions which result from the combination of two different engine speeds (800/1500 rpm) and two different intake pressures (0.4/0.95 bar). The selected experimental dataset is characterized by a revving speed and an intake pressure equal to 800 rpm and 0.95 bar, respectively. Other experimental details (such as wall temperatures measured via thermographic phosphors) are summarized in the Table 2. No experimental data of crevice wall temperature are available; for this reason, the authors have assumed a mean wall temperature of 80°C.
In Fig. 1 a schematic representation of cylinder and ports is shown to point out the positions of the intake/exhaust pressure and temperature sensors (P/T_{MAN} and P/T_{EXH}). The experimental dataset includes a measure of the intake mass flow rate (via a Bronkhorst mass flow controller [27]) and an ensemble average of the in-cylinder pressure as well. All the pressure and temperature data proposed in the present manuscript represent averages over 85 consecutive cycles.

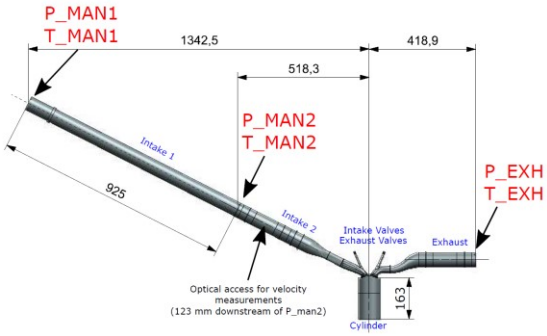

Figure 1**:** Schematic representation of cylinder and ports

Engine features		
Bore	86	mm
Stroke	86	mm
Compression ratio (Ref.)	8.7	
RPM	800	
IVO (ref. 0.1 mm)	340	CA [aTDC]
EVO (ref. 0.1 mm)	120	CA [aTDC]
IVC (ref. 0.1 mm)	590	CA [aTDC]
EVC (ref. 0.1 mm)	375	CA [aTDC]

Table 1: Engine features

Experimental setup				
Intake pressure [bar]	**Intake Temperature [°C]**	**Intake mass flow [Kg/h]**	**Exhaust Pressure [bar]**	**Exhaust Temperature [°C]**
0.95	24	11.36	0.996	35
In-cylinder Wall Temperature [°C]				
Head		**Piston**		**Liner**
70		110		60

Table 2: Experimental data: pressures and temperature reported here come from P_MAN1/T_MAN1 and P_EXH/T_EXH sensors.

3 Numerical setup

1D simulations are carried out with the GT-Power software, licensed by Gamma Technologies. Table 3 and Figure 2 show some details of the 1D model. A simplified description has been used for the modelling of both blow-by and the crevice volume, which makes 1D and 3D domains comparable. In detail, cylinder object is connected to a pipe via an orifice representative of the flow passage area between cylinder and piston crevice. Pipe length is equal to the crevice height. Such pipe is connected via another orifice (whose diameter needs to be calibrated to set the blow-by mass flow rate) to a second duct representing the volume between the seal rings.

Finally, a third orifice leads to the last pipe which should emulate the gap between piston skirt and liner. These additional volumes end in an environment characterized by ambient pressure and temperature (1 bar and 298 K). Thanks to this dedicated modelling, no cylinder object sub-model is used for blow-by and crevice description. Since the piston crevice volume is out of the cylinder, the compression ratio used in the in 1D object is nearly 10 (according to the clearance height of 2.6 mm), rather than the geometric one. In the 3D model, instead, the computational domain includes the crevice, so the compression ratio is 8.7.

1D Model setup		
Environment pressure	0.95	bar
Environment Temperature	23.9	°C
Compression ratio (Cyl)	10.017	
Crevice height	77.6	mm
Heat transfer multiplier (Cyl)	1	
Heat transfer multiplier (Crevice)	1	
Blow-by equiv. diameter	0	mm

Table 3: 1D model base setup

STAR-CD Version	4.30.029
Turbulence Approach	RANS
Turbulence Model	k-ε RNG (High Reynolds)
	Standard k-ε (Low Reynolds)
Heat Transfer Model	GruMo-UniMORE
Numerical Discretization	MARS 0.5

Table 4: Main 3D numerical models

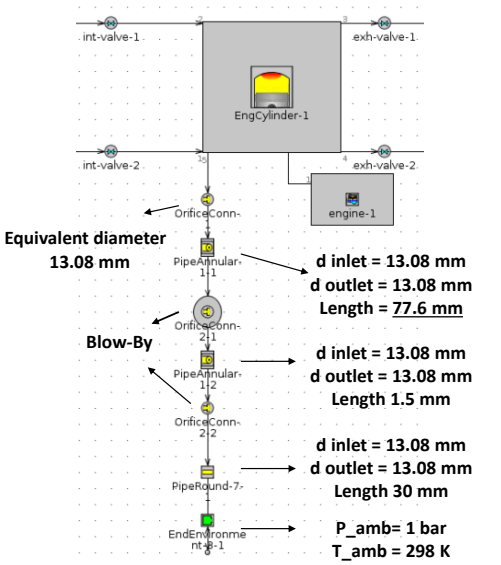

Figure 2: Crevice modelling in 1D model

3D CFD simulations are carried out using the STAR-CD code licensed by SIEMENS PLM. Figure 3a) shows the 3D computational grid at bottom dead center. Total number of cell is 3.6M. Figure 3b) reports the grid at top dead center, where the number of cells decreases up to 2.7M. As for the near-wall grid, two layers are adopted, each one of 0.25 mm according to the High Reynolds approach. Referring to Fig. 2, the 3D CFD domain ends at the first orifice; indeed, according to the 1D geometry, crevice height is 77.6 mm. The latter is discretized with 4 layers in the radial direction. The computational grid shown in fig. 3 has been used also for Low Reynolds case excluding the intake and exhaust manifolds and using 16 wall layers along crevice thickness and 12 cell layers on cylinder walls. The latter has 1.1 M cells at the BDC.

PISO algorithm is used as implicit time integration method. Time step is set to 0.05 CA, except for valve opening and closing timings where 0.02 CA is preferred. All 3D simulations are carried out with RANS turbulence approach and the table 4 summarized the main 3D numerical models used, such as k-ε RNG turbulence model for the High Reynolds cases, the Standard k-ε version for the Low Reynolds ones and the GruMo-UniMORE model for heat transfer modeling [35,36].

Referring to Fig. 1, 3D intake boundary corresponds to "MAN2" position (where experimental sensors are positioned), while the exhaust ones are located at the "EXH" section.

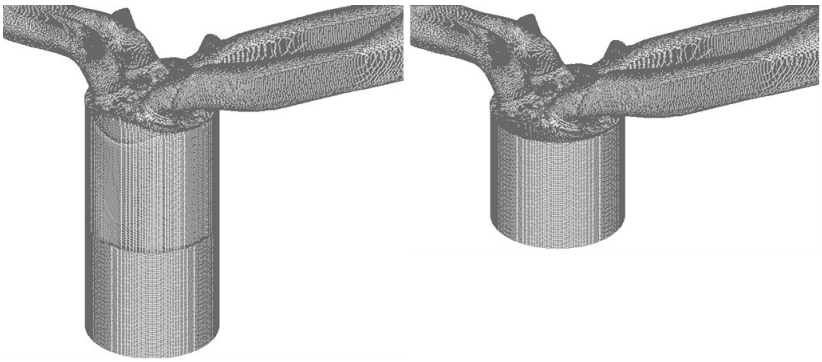

a) **b)**

Figure 3: Computational domain at: a) BDC [@180CA], b) TDC [@360CA]

3 Results

Firstly, a preliminary simulation of the 1D model is carried out. At this stage, the crevice height is kept to 77.6 mm (as indicated by the nominal geometry) and blow-by effect is neglected. The 1D model base setup leads to the pressure traces at the intake and exhaust sections ("MAN2" and "EXH") shown in the fig. 4. A good agreement is noticed compared to the experimental counterparts.

Afterwards, a preliminary 3D simulation with a high-Reynolds wall treatment is carried out using the boundary conditions provided by the 1D model. A 1D-3D comparison is proposed in Fig. 5 and Table 5, in terms of in-cylinder pressure, trapped mass and intake mass flow. 1D and 3D models return a similar mean in-cylinder pressure and both overestimate the experimental peak pressure of nearly two bar (that is 15%), as visible in Fig. 5a). Such overestimation is not due to the trapped mass, in fact for both the models, which are characterized by the same trapped mass, the intake mass flow rate is in agreement with the experiments (the error is nearly 2%).

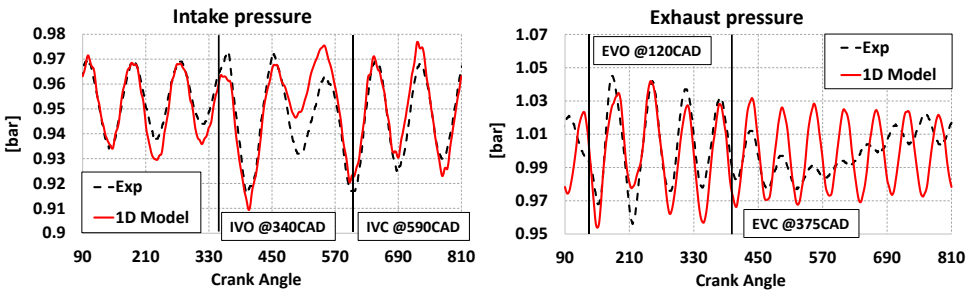

a) **b)**

Figure 4: Pressure at intake and exhaust boundaries.

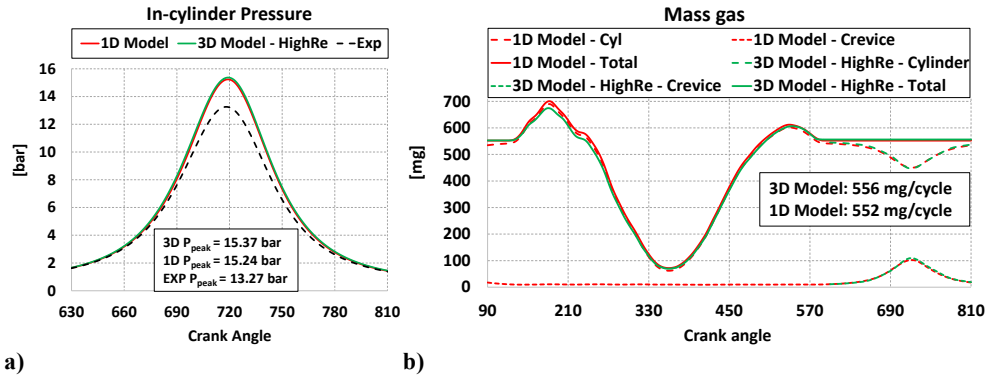

Figure 5: **a)** In-cylinder pressure; **b)** trapped mass

Intake mass flow (Cycle average)		
[Kg/h]		
Exp	**1D Model**	**3D Model High Re**
11.36	11.52	11.63

Table 5 : Intake mass flow

In order to explain the difference between simulations and experiments in terms of pressure, the blow-by effect is investigated at first. To do this, a sweep of equivalent diameters of the first blow-by orifice is considered, thus opening the crevice volume to the environment. The results in terms of in-cylinder pressure are shown in Fig. 6. For small orifice equivalent diameters (lower than 1 mm) the peak pressure variation is reduced; to make the peak pressure comparable with the experimental one, the blow-by diameter has to be increase up to 2 mm. However, in this last case, the alignment during the expansion stroke is completely lost, that is the numerical pressure underestimates the experimental counterpart. This is due to the non-symmetric effect of the blow-by on the pressure trace and therefore the peak pressure is anticipated. As shown in Fig. 5, both 1D and 3D results are characterized by an almost symmetric overestimation of the experimental trace, hence it is necessary to work symmetrically on the pressure.

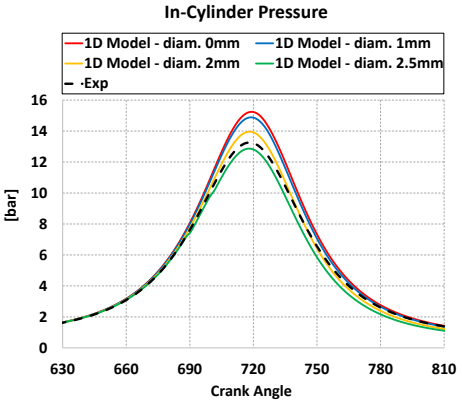

Figure 6: In cylinder pressure for different equivalent diameters of the first blow-by orifice.

In order to avoid non-symmetric effect, the orifice diameter cannot be greater than 1.2 mm, which corresponds to a negligible blow-by. Since such a diameter does not lead to significant improvement on the mean in-cylinder pressure, blow-by is neglected in the present work and the equivalent diameter of the first blow-by orifice is set equal to 0.
The second investigated aspect is the heat transfer. As visible in Fig. 7a), with the present set-up (that is on equal compression ratio and trapped mass and blow-by null) 1D and 3D models show a different heat transfer. In particular, in the 3D high-Reynolds case, the heat exchanged through the crevice walls is double than the one transferred to the cylinder boundaries. Conversely, for the 1D model, values are similar. This is confirmed by the average heat transfer reported in Table 6a) as well. However, despite a different behavior, the two different numerical frameworks provide a similar result in terms of in-cylinder pressure, as visible in Figs. 5a) and 7b).
As no experimental data is available in terms of heat transfer, a dedicated 3D analysis is carried out. A simulation with the Standard k-ε and a low-Reynolds wall treatment is run. Since a low-Reynolds approach allows a proper simulation of the boundary layer (rather than a modeling based on wall functions), the resulting heat transfer can be considered as a reliable estimation for the validation of both 1D and 3D (high-Reynolds) models. The low-Reynolds analysis starts at the intake valve closing and ends at exhaust valve opening, so that only the cylinder is included in the simulation domain. Observing, in Fig. 7a), the outcomes provided by the low-Reynolds analysis, it emerges that both 1D and 3D (high-Reynolds) cases underestimate the heat flux through the cylinder walls. This is, at least partially, the reason of the misalignment between numerical results and experiments. As a proof of this, in the Low-Reynolds case the overestimation of pressure reduces as visible in Fig. 7b). As for the 1D model, predictive capabilities in terms of heat transfer are limited, thus a tuning of the convective heat transfer multiplier (HT) is usually needed as in this case.

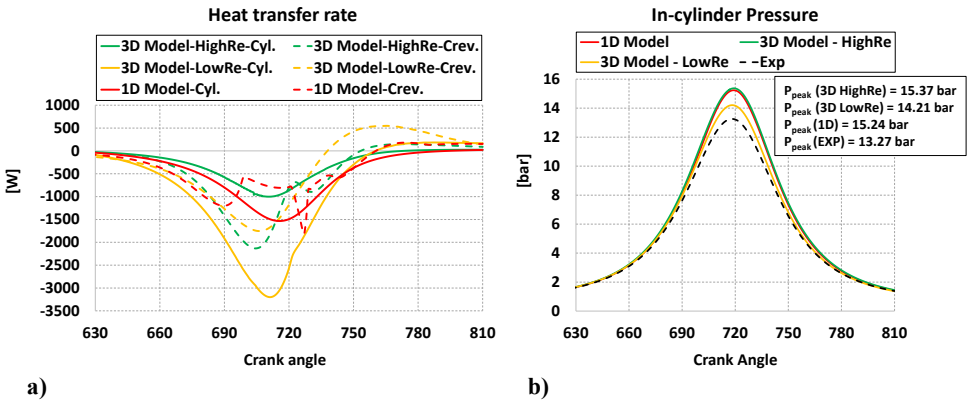

Figure 7: **a)** Heat transfer rate through cylinder and crevice walls during compression and expansion strokes; **b)** In-cylinder pressure

As for the 3D model, limitations of a high-Reynolds wall treatment is clearly pointed out in [37-39]. In complex flows such as the in-cylinder ones, dimensionless profiles of u+ and T+ are usually far from standard wall functions. Therefore high-Reynolds wall treatments, which rely on laws of the wall, provide poor estimations of the heat transfer. As a consequence, a tuning of the latter is required for the 3D model as well. However, the tuning is carried out only for the cylinder since, for the crevice, the high-Reynolds wall

treatment is able to provide a reliable estimation of the heat transfer. This is due to the fact that the flow in the crevice fulfill the requirements for the existence of profiles comparable to wall functions. Such considerations are confirmed by the average heat transfer during the hot portion of the engine cycle, reported in Table 6b). The high-Reynolds wall treatment deeply underestimates the average heat transfer through the cylinder walls. Conversely, at the crevice, just a slight overestimation can be noticed, which is probably a consequence of the reduced heat fluxes through the cylinder.

Average Heat Transfer Rate [W]		
	1D Model	3D Model HighRe
Cylinder	83	42.8
Crevice	93	115.6

a)

Average Heat Transfer Rate [W]		
[600-810 CAD]		
	3D Model HighRe	3D Model LowRe
Cylinder	250	737
Crevice	417	298

b)

Table 6: Average heat transfer rate: a) comparison between 1D and 3D models (full cycle); b) comparison between high-Reynolds and low-Reynolds wall treatments (during the closed-valve portion of the engine cycle).

In order to improve the heat transfer estimation provided by the high-Reynolds wall treatment, a new case is run using a multiplier equal to 6 for the heat transfer coefficients at the cylinder walls. As for the crevice volume and intake/exhaust ports, no modification is accounted for. New outcomes in terms of in-cylinder pressure and heat transfer are shown in Fig. 8, where original cases are included for comparison.
As shown in Fig. 8a and 8b, the modified high-Reynolds simulation (HT Mod.) is in good agreement with the corresponding low-Reynolds outcomes. The same is valid in terms of average wall heat transfer as well, as visible in Table 7. Only a reduced underestimation still remains at the cylinder boundaries (~ 100 W), while a negligible difference (~30 W) can be observed for the crevice. At the latter, despite no multiplier was adopted, a remarkable reduction of the heat transfer is obtained (~ 100 W), because of the higher heat fluxes through the cylinder walls which lower the gas temperature.

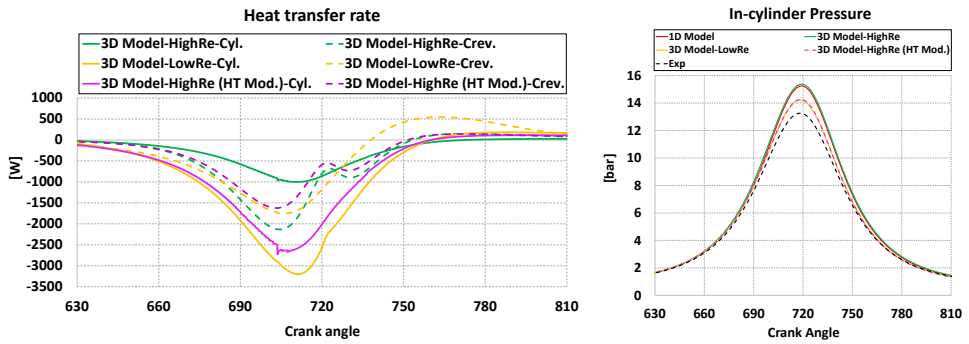

a) **b)**

Figure 8: **a)** Heat transfer through cylinder and crevice walls during the closed-valve portion of the engine cycle; **b)** In-cylinder pressure

3D - Average Heat Transfer Rate [W]			
	600 ÷ 810 CA [aTDC]		
	3D Model LowRe	**3D Model HighRe**	**3D Model HighRe (HT Mod.)**
Cylinder	737	250	636
Crevice	298	417	325

Table 7: Average heat transfer rate during closed valves cycle phase of HighRe and LowRe 3D models

However, the most important improvement is noticed in terms of mean in-cylinder pressure. As visible from Fig. 8b), thanks to the tuning of the heat transfer, the in-cylinder pressure of the high-Reynolds simulation is not only able to match the low-Reynolds counterpart, but it is also prone to the experimental one. Since the heat transfer provided by the low-Reynolds approach represents a reference for the 1D model as well, the latter was accordingly modified via the cylinder object multiplier. Fig. 9 reports the results for the 1D model along with the ones provided by the 3D simulations for comparison. Thanks to the ad hoc tuning, the 1D model aligns with the corresponding 3D one.

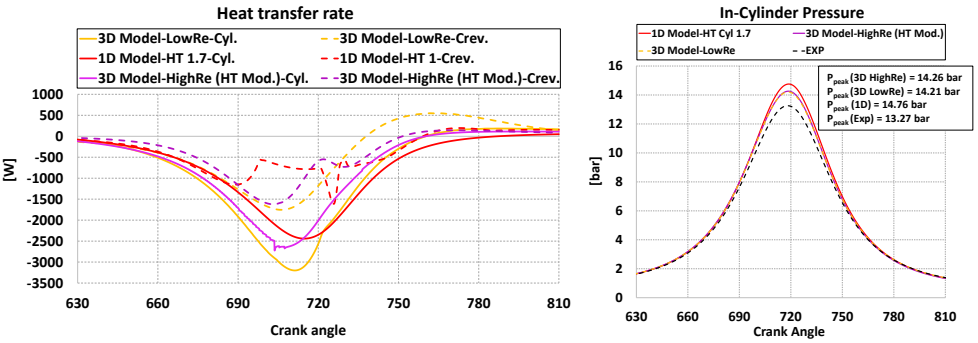

Figure 9: **a)** Heat transfer rate through cylinder and crevice walls during closed valves cycle phase; **b)** In-cylinder pressure.

However, as visible from Figs. 9a) and 9b), a difference in terms of timing can be noticed between 1D and 3D simulations, leading to a slight misalignment of pressure peak. The reason of the different heat transfer timing is due to the simplified default model adopted in GT-Power [40], which is not able to account for local phenomena of the boundary layer
It is important to highlight that a proper tuning of the heat transfer leads to further improvement of the results in terms of intake mass flow rate. In this case, as reported in Table 8, both 1D and 3D models fairly reproduce the experimental data. From Fig. 9b) it emerges that a difference still remains between numerical simulations and experiments, despite all the involved aspects (i.e. trapped mass, blow-by and heat transfer) were investigated and the compression ratio is equal to the nominal one.
As for the latter, experimental uncertainties must be expected. It is interesting to point out that small modification of the compression ratio, in the order of 5%, brings to a result very close to experimental one. Therefore, assuming such an uncertainty of the engine geometry, the crevice height is increased to 101mm obtaining a new compression ratio equal to 8.23 (instead of 8.7). The latter is adopted both in 1D and 3D models and the resulting in-

cylinder pressure traces are shown in Fig. 10. As visible, both the numerical frameworks fairly reproduce the experimental curve.

Intake mass flow (Cycle average)		
[Kg/h]		
Exp	**1D Model (HT 1)**	**3D Model High Re HT Mod.**
11.36	11.43	11.38

Table 8 : Intake mass flow of experiment, 1D and 3D models

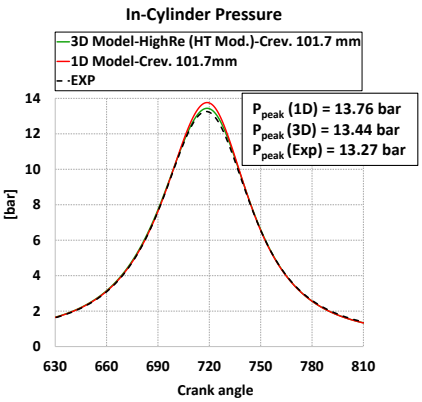

Figure 10: In-cylinder pressure.

4 Conclusions

In the present paper, a preliminary validation of both 1D and 3D models of the Darmstadt optical research engine is carried out against experimental data under motored condition. The selected operating point is characterized by a revving speed of 800rpm and intake pressure and temperature equal to 950 mbar and 24 °C, respectively. Since numerical frameworks clearly demonstrated to widely overestimate the in-cylinder pressure, different involved phenomena were investigated such as blow-by and heat transfer, with the aim to reduce the gap compared to the experimental data.
The first analysis is carried out using the 1D model to evaluate the impact of the blow-by, which is found to be negligible for the present analysis. Afterwards, a detailed investigation on the heat transfer via a 3D low-Reynolds simulation has allowed a proper tuning of the heat fluxes of both 1D and 3D (high-Reynolds) models. Despite the reduction of the uncertainties in terms of blow-by and heat transfer, a non-negligible overestimation of the mean in-cylinder pressure still remains. In order to improve the agreement with the experimental data, a small variation of the compression ratio is accounted for, justified by the uncertainty related to its evaluation. Thanks to an ad-hoc modification of the crevice height, a proper estimation of both the in-cylinder pressure and the intake mass flow rate by 1D and 3D models is obtained.

References

1. Yong, Jia Ying & Ramachandaramurthy, Vigna K. & Tan, Kang Miao & Mithulananthan, N., 2015. Renewable and Sustainable Energy Reviews, Elsevier, vol. 49(C):365-385. DOI: 10.1016/j.rser.2015.04.130
2. V. Mangeruga, M. Giacopini S. G. Barbieri, F. Berni, E. Mattarelli, C. A. Rinaldini, SAE Int. J. Adv. & Curr. Prac. in Mobility 2(2):721-736, 2020, https://doi.org/10.4271/2019-24-0197.
3. L. Teodosio, F. Bozza, F. Berni, (2019) AIP Conference Proceedings, 2191(1). https://doi.org/10.1063/1.5138880
4. L. Teodosio, V. De Bellis, F. Bozza, D. Tufano, (2017), SAE International. https://doi.org/10.4271/2017-24-0015

5. E. Severi, A. d'Adamo, F. Berni, S. Breda, M. Lugli, E. Mattarelli, (2015) Energy Procedia 81:p. 846-855, https://doi.org/10.1016/j.egypro.2015.12.094
6. L. Teodosio, V. De Bellis, F. Bozza, *SAE Int. J. Engines* 11(6):643-656, 2018, https://doi.org/10.4271/2018-01-0854.
7. L. Teodosio, D. Pirrello, F. Berni, V. De Bellis, R. Lanzafame, A. d'Adamo, (2018) Applied Energy, 216: p. 91-104. https://doi.org/10.1016/j.apenergy.2018.02.032
8. F. Berni, S. Breda, A. d'Adamo, S. Fontanesi, G. Cantore, SAE Technical Paper 2015-24-2499, 2015, DOI:10.4271/2015-24-2499
9. S. Breda, F. Berni, A. d'Adamo, F. Testa, E. Severi, G. Cantore, (2015) Energy Procedia 82:p. 96-102, DOI: 10.1016/j.egypro.2015.11.888
10. S. Breda, F. D'Orrico, F. Berni, A. d'Adamo, S. Fontanesi, A. Irimescu, S.S. Merola, Fuel, 243:p.104-124, https://doi.org/10.1016/j.fuel.2019.01.111.
11. L. Postrioti, A. Cavicchi, G. Brizi, F. Berni, S. Fontanesi, SAE Technical Paper 2018-01-0271, 2018, https://doi.org/10.4271/2018-01-0271.
12. V. K Krastev, A. d'Adamo, F. Berni, S. Fontanesi, (2019) International Journal of Engine Research 21(1), DOI: 10.1177/1468087419851905
13. F. Bozza, V. De Bellis, F. Berni, A. d'Adamo, L. Maresca, SAE Technical Paper 2018-01-0850, 2018, https://doi.org/10.4271/2018-01-0850.
14. E. Mattarelli, M. Borghi, D. Balestrazzi, S. Fontanesi, SAE Technical 2004-01-0112, (2004), https://doi.org/10.4271/2004-01-0112.
15. G. Bianchi, S. Fontanesi SAE TRANSACTIONS. 112-3(2003), pp. 29-44. http://dx.doi.org/10.4271/2003-01-0003
16. M. D. Ribeiro, A. M. Bimbato, M. A. Zanardi, J. A. Perrella Balestieri, D. P. Schmidt, (2020) International Journal of Engine Research 1-22. https://doi.org/10.1177/1468087420903622
17. S. Sparacino, F. Berni, A. Cavicchi, L. Postrioti, (2019) AIP Conference Proceedings 2191(1), DOI: 10.1063/1.5138872
18. S. Sparacino, F. Berni. A. d'Adamo, V. K. Krastev, A. Cavicchi, L. Postrioti, (2019) Energies, 12 (15), art. no. 2890, DOI: 10.3390/en12152890
19. C. Geschwindner, P. Kranz, C. Welch, M. Schmidt, B. Bohm, S. A Kaiser, J. De la Morena, (2019) International Journal in Engine Research 1-16, DOI: 10.1177/146887419881535.
20. Y. Shekhawat, D.C. Haworth, A. d'Adamo, F. Berni, S Fontanesi, P. Schiffman, D. Reuss, V. Sick, (2017) Oil and Gas Science and Technology, 72(5). DOI: 10.2516/ogst/2017028
21. A. d'Adamo, S. Breda, F. Berni, S. Fontanesi, (2018) SAE International Journal of Engines, 12(1): p. 1-22. DOI: 10.4271/03-12-01-0007
22. A. d'Adamo, S. Breda, S. Iaccarino, F. Berni, S. Fontanesi, B. Zardin, M. Borghi, A. Irimescu, S. S. Merola, (2017), SAE International Journal of Engines 10(3). DOI: 10.4271/2017-01-0551
23. A. d'Adamo, S. Breda, F. Berni, S. Fontanesi, (2019) Applied Energy 249:126-142. DOI:10.1016/j.apenergy.2019.04.093
24. A. Rosetti, C. Iotti, A. Bedogni, G. Cantore, S. Fontanesi, F. Berni, (2019) SAE Technical Papers 2019-24-0006, DOI: 10.4271/2019-24-0006
25. I. Ko, K. Min, F. Rulli, A. d'Adamo, F. Berni, S. Fontanesi, SAE Technical Papers, 2017-24-0040 (2017). DOI: 10.4271/2017-24-0040
26. F. Rulli, S. Fontanesi, A. d'Adamo, F. Berni, (2019) International Journal of Engine Research. DOI: 10.1177/1468087419836178
27. E. Baum, B. Peterson, B. Bohm, A. Dreizler, (2014) Flow Turbulence Combustion, 92(1-2), DOI:10.1007/s10494-013-9468-6.
28. S.H.R. Muller, B. Bohm, M. Gleibner, R. Grzeszik, S. Arndt, A. Dreizler, (2009) Research Article, Experiments in Fluids 48(2):281-290. DOI 10.1007/s00348-009-0742-2.
29. D. Freudenhammer, B. Peterson, C-P. Ding, B. Bohm, S. Grundmann, (2015) SAE International Journal of Engines 8(4), DOI:10.4271/2015-01-1697.
30. G. Cicalese, F. Berni, S. Fontanesi, A. d'Adamo, E. Andreoli, SAE Technical Papers, 0148-7191, (2017). DOI: 10.4271/2017-01-2196
31. G. Cicalese, F. Berni, S. Fontanesi, (2016) SAE International Journal of Engines 9(1):609-625. DOI: 10.4271/2016-01-0578
32. S. Fontanesi, G. Cicalese, G. Cantore, A. d'Adamo, SAE Technical Paper 2014-01-1151, 2014. https://doi.org/10.4271/2014-01-1151.

33. A. Irimescu, C. Tornatore, L. Marchitto, S. S. Merola, (2013) Applied Thermal Engineering 61(2) 101-109. DOI:10.1016/j.applthermaleng.2013.07.036
34. C. Welch, M. Schmidt, K. Keskinen, G. K. Giannakopoulos, K. Boulouchos, A. Dreizler, B. Bohm, SAE Technical Paper 2020-01-0792, 2020, https://doi.org/10.4271/2020-01-0792
35. F. Berni, G. Cantore, S. Fontanesi, (2017), Applied Thermal Engineering 115:1045-1062. https://doi.org/10.1016/j.applthermaleng.2017.01.055.
36. G. Cicalese, F. Berni, S. Fontanesi, (2016) SAE International Journal of Engines 9(1):609-625. DOI: 10.4271/2016-01-0578
37. F. Berni, S. Fontanesi, G. Cantore, A. d'Adamo, (2017) SAE International Journal of Commercial Vehicles 10(2):547-561, https://doi.org/10.4271/2017-01-0569.
38. F. Berni, S. Fontanesi, (2020) Applied Thermal Engineering, vol.174 DOI: 10.1016/j.applthermaleng.2020.115320
39. F. Berni, G. Cantore, S. Sparacino, G. Cantore (2019) AIP Conference Proceedings 2191,020019. https://doi.org/10.1063/1.5138752
40. GT-Power Modelling User guided version.

Acknowledgments

The authors want to thank the DARMSTADT Research Group for providing experimental data and the 1D model.